JOURNAL OF MATERIALS SCIENCE **36** (2001) 49–54

Amorphous phase formation of Zr-based alloy coating by HVOF spraying process

H. J. KIM*
RIST, P.O. Box 135, Pohang, Korea 790-600
E-mail: khyungj@rist.re.kr

K. M. LIM
POSTECH, Department of Mat. Sci. and Eng., Pohang, Korea 790-784

B. G. SEONG
RIST, P.O. Box 135, Pohang, Korea 790-600

C. G. PARK
POSTECH, Department of Mat. Sci. and Eng., Pohang, Korea 790-784

This investigation was conducted to clarify the effects of process parameters on the formation of the new amorphous coating using a Zr-based alloy, which is known as bulk metallic glass forming alloy, by a HVOF (High Velocity Oxygen Fuel) spraying process. Powders used for spraying was prepared by vacuum gas atomization and then crushed by a centrifugal mill. HVOF spraying experiments were carried out using a Tafa JP-5000 spraying gun. DTA (Differential Thermal Analysis) measurements have shown that the amorphous content of the coatings was measured up to about 62% depending on the spraying process parameters. The amorphous fraction of the coatings is decreased with increasing the spray distance and the fuel flow rate. Microstructural observations and X-ray diffraction analysis of the spray coated layers reveal that the amorphization behavior during the spraying is attributed to the degree of the solidification of droplets and the oxide (ZrO_2) formation in spray coated layers. Therefore, flame temperature and spray distance that can control the carrier gas temperature and undercooling effects of the droplets are the most crucial factors for the evolution of the amorphous phase using this bulk metallic glass forming alloy.

1. Introduction

Significant interest has been generated in amorphous alloys due to their unique physical, mechanical, and chemical properties. It is also of great interest to exploit the excellent mechanical properties and corrosion resistance of amorphous alloys in the form of protective coatings. Consequently, a variety of technologies have been used to produce such coatings [1]. Thermal spraying is probably the most economical method for the production of thick (0.05–2 mm) amorphous surface layers [2–6]. However, few successful thermal sprayed coatings have been developed and commercialized since it is difficult to produce fully amorphous structure in air. Furthermore, thermal sprayed coatings with partially amorphous structure do not give anticipated excellent protection on wear and corrosion since defects such as lamellar structure and pores which are unique in thermal sprayed coatings overwhelm the beneficial effects of amorphous structure [7].

Most of previous investigations have worked with Fe- and Ni-based alloys with eutectic composition containing metalloid such as B, Si, and C [1–5, 8, 9]. Although it was reported that the initial powder state has little or no influence on the amorphous content of the coatings [1], utilizing the fully amorphous powders increases the amorphous content of the coatings since the HVOF (High Velocity Oxygen Fuel) spraying frequently contains unmelted particles. It is also expected that utilizing the HVOF spraying may prevent the formation of the oxide phase in the coating since the atmosphere of the HVOF spraying is reducing rather than oxidizing.

Recently, it has been discovered that special multicomponent alloys can form amorphous structure with much slower cooling rate (around 100 K/sec) during solidification than conventional alloys [10–12]. It is known that the cooling rate required for the formation of amorphous structure of conventional alloys is usually higher than 10^5 K/sec. These alloys with high glass forming ability are called BMG (Bulk Metallic Glass) alloys.

This article reports on the amorphous phase formation of Zr-based BMG forming alloy by HVOF spraying. This is a new approach (probably the first approach)

* Author to whom all correspondence should be addressed.

that the BMG forming alloy is studied for the amorphous coating by thermal spraying.

2. Experimental details

2.1. Preparation of the powders for spraying

One of the well-known BMG alloys, $Zr_{65}Al_{7.5}Ni_{10}Cu_{17.5}$ (at. %), was used for this investigation. Master alloy was produced with 98.5% Zr and 99.99% Al, Ni, and Cu granules by the arc melting furnace. The preparation of the powders for spraying was done by vacuum gas atomization. The details of the vacuum gas atomization are reported elsewhere [13]. Since the average size of the powders produced by vacuum gas atomization was above 130 μm, the powders were sieved to 20–90 μm after crushed by centrifugal mill. Thus, the shape of the powders is not spherical as shown in Fig. 1a. Cross sectional examination of the powders reveals that the powders are the mixture of crystalline and amorphous structure as shown in Fig. 1b. Table I shows the compositions of the target and powders prepared for spraying. Although the composition of the powders deviate from the target one, the critical cooling rate for glass forming of the powders prepared is still around 100 K/sec [10, 12]. It is also noted that the powders prepared for spraying are already contaminated by oxygen resulting from the centrifugal milling process.

TABLE I Chemical compositions (at. %) of the powders and the coatings studied

Composition (at. %)	Zr	Al	Ni	Cu	O
Target	65	7.5	10	17.5	—
Powders for spraying	62.0	8.3	8.8	17.0	3.6
Coating	61.0	7.8	8.0	12.8	10.0

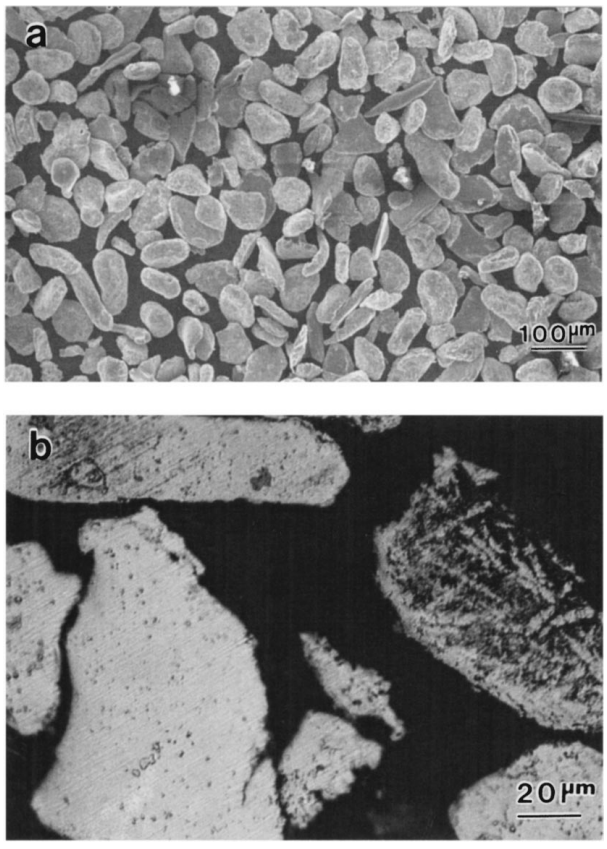

Figure 1 The powders for spraying prepared by vacuum gas atomization and crushed by centrifugal mill. (a) Scanning electron micrograph showing the morphology of the powders. (b) Optical micrograph of the etched cross-section of the powders showing both the amorphous and the crystalline structures.

TABLE II Experimental conditions of the HVOF spraying using a Tafa JP5000 gun

Spray parameters	Spray conditions
Oxygen flow rate (SCFH)	1500
*Fuel flow rate (GPH)	2.0, 2.5, 3.5 (F1, F2, F3)
Combustion (psi)	91
Powder gas flow rate (SCFH)	26
Powder feed rate (rpm)	100
Barrel (inch)	4
*Spray distance (mm)	200, 300, 400, 500 (D1, D2, D3, D4)

*When varying the fuel flow rate and the spray distance, the fuel flow rate and the spray distance were fixed to 3.0 GPH and 300 mm, respectively.

2.2. Spraying conditions

HVOF spraying experiments were conducted using a Tafa JP5000 system. Fuel used was Kerosene and the substrate was SUS 304 with a thickness of 4 mm. The substrate was not blasted prior to spraying in order to detach the coatings easily for thermal analysis. Experimental conditions investigated are shown in Table II. When varying the fuel flow rates, the spray distance was fixed to 300 mm. Alternatively, when varying the spray distance, the fuel flow rate was fixed to 3.0 GPH (Gallon Per Hour). The thickness of the coatings produced was 150–200 μm.

2.3. Characterization of the coatings

The thermal properties (the glass transition temperature, the crystallization temperature, and the crystallization enthalpy) of the powders and the coatings were investigated using a Differential Thermal Analyzer (DTA, Perkin Elmer DTA-7). DTA analysis was conducted using a heating rate of 10°C/min up to 800°C. The weight fraction of the amorphous phase ($R_{\text{amorph.}}$) in the coatings or powders is calculated by

$$R_{\text{amorph.}} = \frac{\Delta H_{\text{coating}}}{\Delta H_{\text{ref}}} \quad (1)$$

Where $\Delta H_{\text{coating}}$ is the crystallization enthalpy of the coating measured and ΔH_{ref} is the crystallization enthalpy of the fully amorphous reference sample. It is noted that a similar relationship was found using a X-Ray Diffractometer (XRD), but for volume fraction [2]. The powders below 26 μm produced by vacuum gas atomization in this investigation are regarded as the fully amorphous reference sample [13].

The microstructure of the coatings was examined by optical microscopy and Scanning Electron Microscopy (SEM) equipped with EDS (Energy Dispersive Spectroscopy). Etching of the coatings was conducted using a solution of 0.5% HF for about

30 seconds. The oxide area fraction and the porosity (% area) of the coatings were measured by image analyzer at a magnification of 500. About 40 measurements of each sample were conducted to have the average value of the coatings. The phase analysis was conducted using a XRD with a Cu K_α target. The scanning rate was 1°/min for 2θ range of 20–90°.

3. Results and discussion

3.1. Microstructural evaluation

Fig. 2 shows the cross sectional microstructures of the sprayed coatings with a variation of the fuel gas flow rates. As the fuel gas flow rate is increased, the microstructure of the coatings tends to be more compact, that is, less pores and thinner lamellae thickness.

Fig. 3 shows the etched cross sectional microstructures of the sprayed coatings with a variation of the spray distance. This time, as the spray distance is increased, the microstructure of the coatings shows a tendency of more pores and thicker lamellae thickness. The results of the quantitative measurements of pores

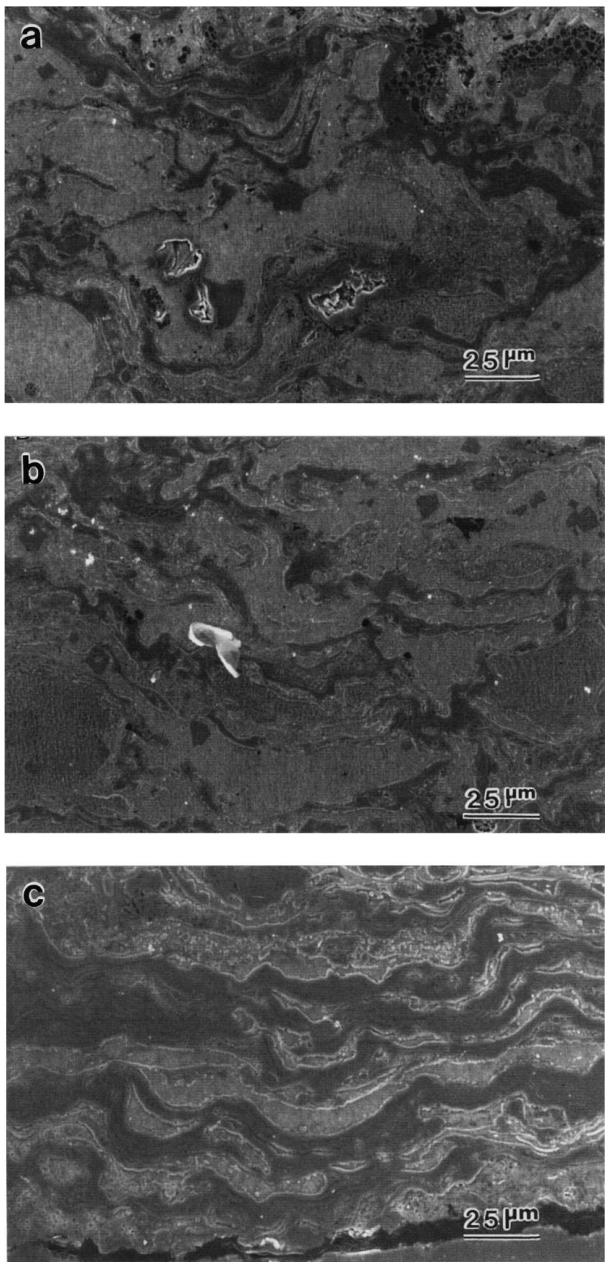

Figure 2 SEM micrographs showing the cross sectional microstructure of the coatings sprayed with different fuel gas flow rates. (a) F1 (b) F2 (c) F3.

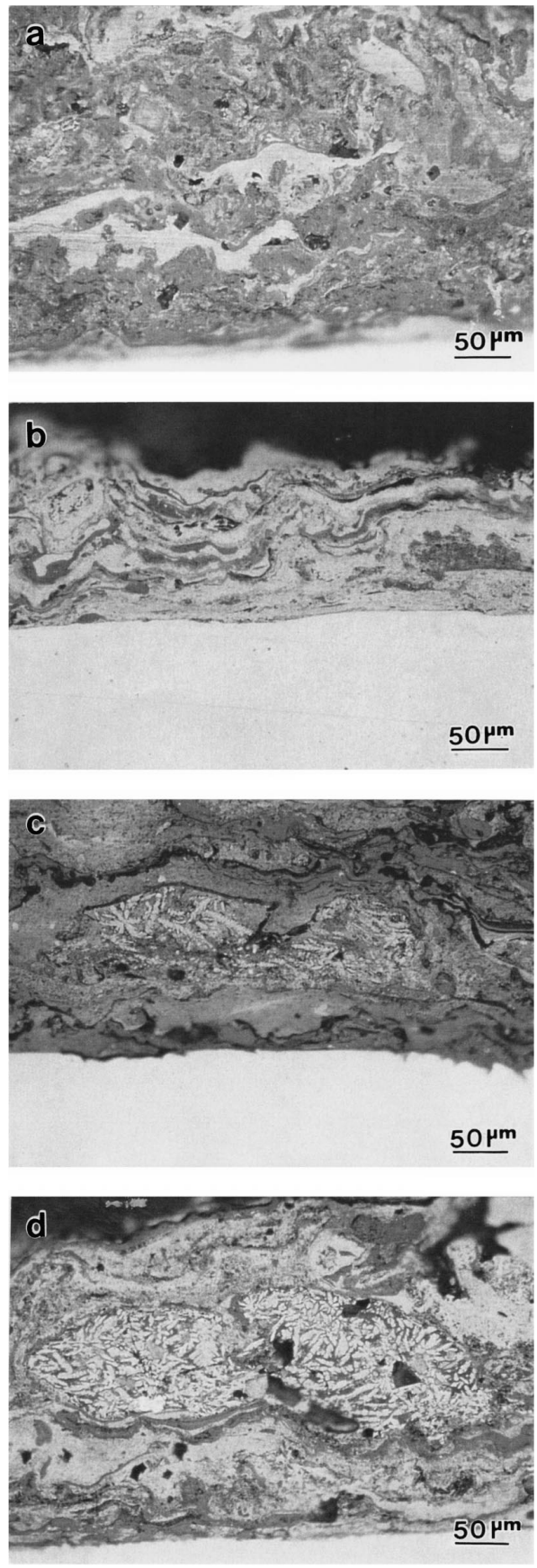

Figure 3 Optical micrographs of the etched cross section of the coatings sprayed with different spray distances. (a) D1 (b) D2 (c) D3 (d) D4.

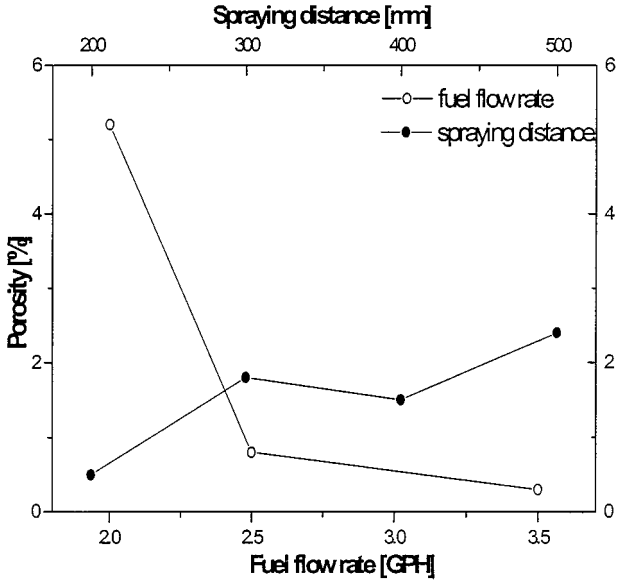

Figure 4 Porosity variations of the sprayed coatings with different fuel gas flow rates and spray distances.

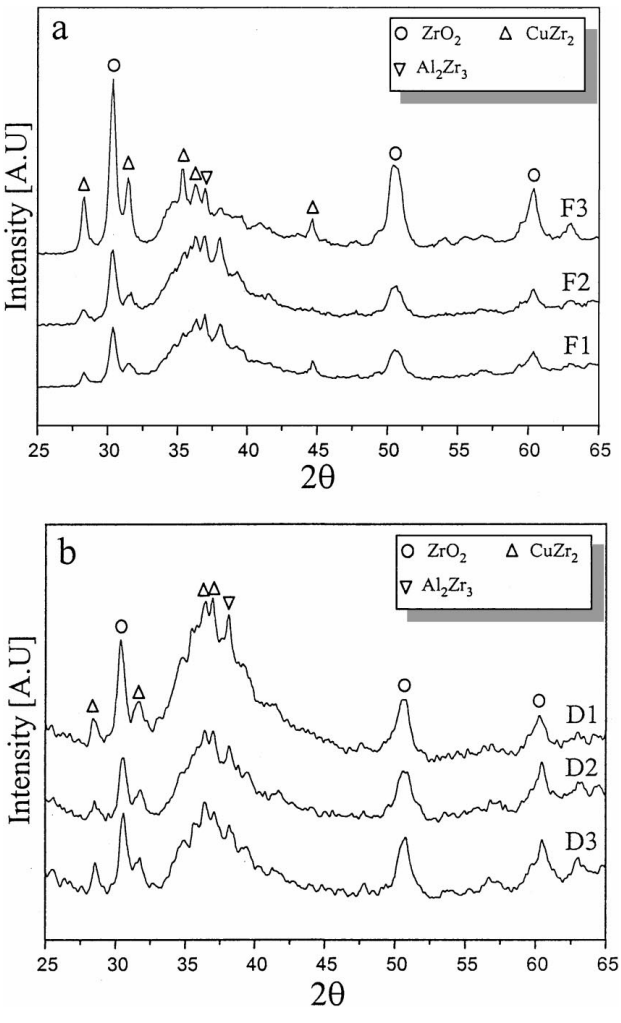

Figure 5 XRD spectra of the sprayed coatings with (a) different fuel gas flow rates and (b) different spray distance.

by image analysis are shown in Fig. 4. It is shown that as the fuel gas flow rate is increased and the spray distance is decreased, the porosity of the coatings is decreased.

Fig. 5 shows the XRD patterns of the as-sprayed coating surfaces. They show almost identical patterns

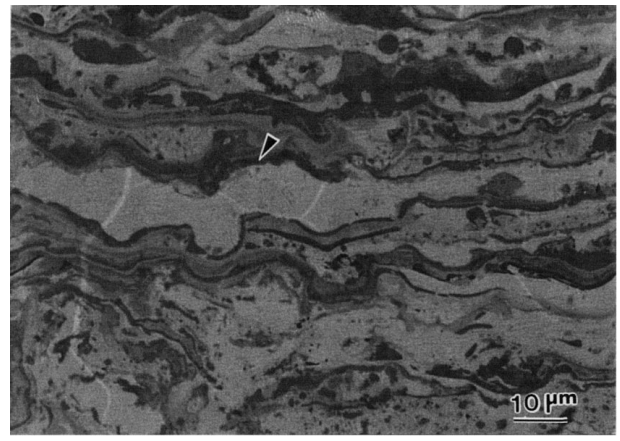

Figure 6 Back scattered electron image of the cross section of the coating.

except F3 coating with rather lager oxide peaks (ZrO_2). All of the diffraction patterns show oxide peaks and hallow patterns that are typical of amorphous structure. Some samples contain crystalline peaks that are identified to $CuZr_2$ and Al_2Zr_3.

Back scattered electron image of the coating is shown in Fig. 6. X-ray elemental mapping of the oxygen confirms that the oxygen is concentrated at the dark region as indicated by the arrow in Fig. 6. EDS analysis of dark regions shows that the oxide phase is mainly from Zr.

The results of quantitative measurements of oxide phase in sprayed coatings are shown in Fig. 7. The oxide area fractions of F1 and F2 samples are similar, while that of the F3 sample is the highest and over 50% as expected from Fig. 5a. The coating sprayed with the shortest spray distance (200 mm) shows the highest oxide fraction with over 50% among the coatings investigated.

The reduction of oxide phase with increasing the spray distance is attributed to the reduction of HVOF flame temperature. The example of the HVOF flame temperature for Mo droplet is reported in Reference 14.

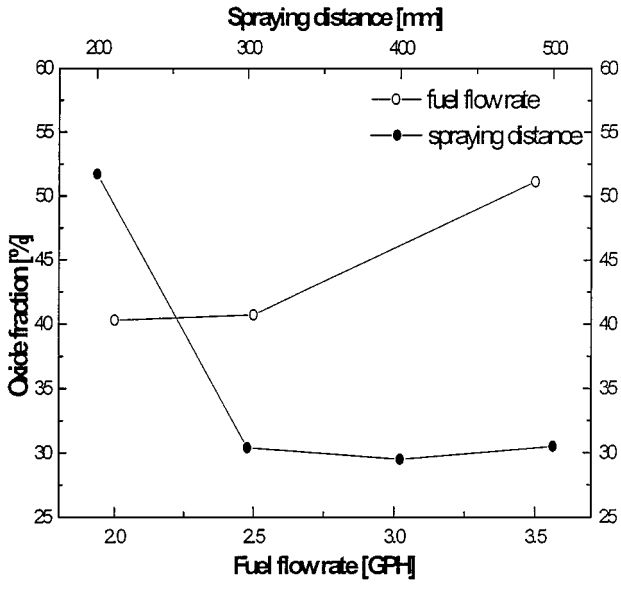

Figure 7 Variations of the oxide fraction (% area) in spray coatings with different fuel flow rates and spray distances.

It was observed that the flame temperature of HVOF jet is significantly decreased in the range of 200–300 mm. Furthermore, HVOF jet flame directly contacts the coating surface when the sample is sprayed at 200 mm spray distance. That is why the oxide fraction of the coating is significantly decreased in the spray distance between 200 mm and 300 mm. Similarly, significant increase of the oxide fraction of the coating with the highest fuel gas flow can be attributed to the highest HVOF flame temperature that the coating is exposed to more high temperature oxidation environments.

3.2. Thermal properties and amorphous fraction of the coatings

Fig. 8 shows the result of DTA measurement for D3 coating as an example. It is noted that all of the coating samples have shown the almost identical DTA curves except an exothermic peak height and/or area. Glass transition temperature (T_g) and crystallization temperature (T_x) are observed around 384°C and 433°C, respectively. Thermal properties of the coating are summarized and compared with the same composition alloy made by the casting in Table III. T_x of the coatings is lower than those of the powders for spraying and the bulk metallic glass. It is also noted that ΔT_x ($T_x - T_g$) of D3 coating is about 50°C which is much lower than that (≅90°C) of the bulk metallic glass. This higher tendency of crystallization of the coatings is attributed to the fact that the chemical compositions of the coatings have changed during spraying as indicated in Table I. Furthermore, the oxygen content of the coatings (see Table I) is much higher than that of the bulk metallic glass alloy resulting from the feedstock powders and the spraying process. It should be also noted

TABLE III Thermal properties of the ZrAlNiCu amorphous alloy prepared by the casting and the thermal spraying

Specimen	T_g (°C)	T_x (°C)	ΔH_x (J/g)	Ref.
Bulk metallic glass (casting)	382	473	56.3	[15]
Powders for spraying	—	441	51.3	This study
Sprayed coating (D3)	384	433	42.5	This study

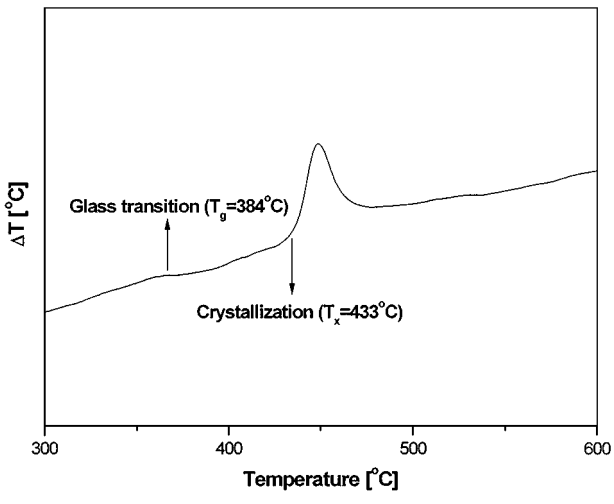

Figure 8 The example of the DTA trace for sprayed coating (D3) studied.

TABLE IV The crystallization enthalpy of the sprayed coatings studied. Symbols of the specimens can be found in Table II

Specimen	Crystallization enthalpy (J/g)
F1, F2, F3	34.5, 33.8, 25.5
D1, D2, D3, D4	31.6, 50.2, 42.5, 41.5
100% amorphous powder	80.6

that a single crystallization peak is observed as features of both eutectic and polymorphous crystallization in contrast to two-step crystallization process (primary crystallization) [16, 17].

Table IV lists the crystallization enthalpy of the coatings and powders measured by DTA and Fig. 9 shows the amorphous contents of the coatings calculated by Equation 1. First of all, as the fuel flow rate is increased, the amorphous content of the coatings is decreased. This is due to the facts that the oxide formation of the coatings has increased at higher HVOF jet temperature as the fuel flow rate is increased.

As far as the spray distance is concerned, D2 coating (300 mm spray distance) shows the highest amorphous content (approximately 62%). At the shortest spray distance (D1 coating), the amorphous content of the coating drops significantly below 40%. This is attributed to the high oxide content (see Fig. 7) since the coating surface is directly exposed to high temperature due to the HVOF jet flame during spraying. Above 300 mm spray distance, as the spray distance is increased, the amorphous content of the coatings is decreased. It is also considered that the formation of the oxide phase has occurred during and/or after solidification of the droplets after molten droplets contact the substrate rather than during the flight since the HVOF jet is a reducing atmosphere.

It is clear that the coatings studied are the mixture of the crystalline, amorphous, and oxide phases from the results of XRD, DTA, and microstructural observations. Therefore, the content of the amorphous phase in the coatings could be determined by the relative amounts

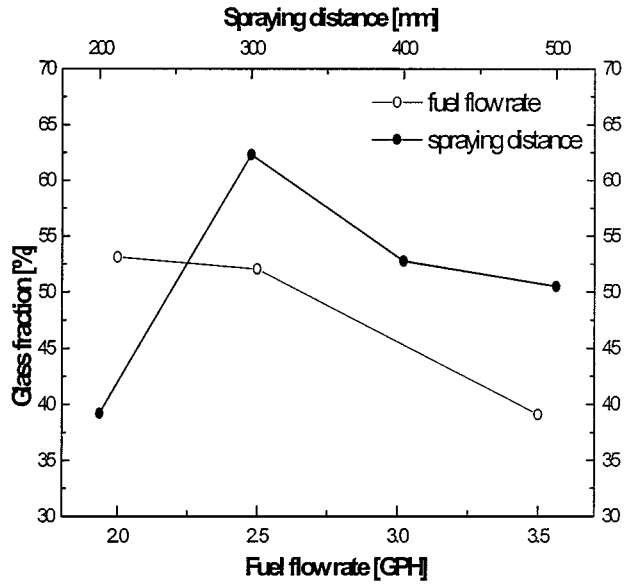

Figure 9 The variations of the amorphous phase fraction (% area) in spray coatings with different fuel flow rates and spray distances.

of the crystalline and oxide phases. Etched cross section of the coatings (see Fig. 3) reveals the crystalline phase clearly. While it is difficult to find the crystalline phase for D1 and D2 coatings, it is easy to observe the crystalline phase for D3 and D4 coatings. It is observed that D4 coating contains more crystalline phase than D3 coating although it has not been measured quantitatively. Therefore, it is considered that the reduction of the amorphous content of the coatings with increasing the spray distance above 300 mm results from the evolution of the crystallization phase due to high degree of supercooling with decreasing temperature.

The amorphous content of the feedstock powders prior to spraying process is approximately 64% from Tables III and IV. The maximum amorphous content of the coatings studied is around 62%. Therefore, it is shown that it is feasible to produce the fully amorphous coating for BMG forming alloy with proper HVOF spraying processing parameters if the fully amorphous powders for spraying are prepared.

4. Conclusions

The Zr-based BMG alloy was sprayed by HVOF spraying, and the variations of the amorphous content and oxide fraction of the coatings with different spraying parameters were measured quantitatively. The main results are as follows:

(1) Maximum amorphous content of the Zr-based BMG alloy studied was measured up to approximately 62% at spray distance of 300 mm by HVOF spraying. It is considered that the reduction of the amorphous content of the coatings with increasing the spray distance results from the evolution of the crystallization phase due to high degree of solidification with decreasing temperature. On the other hand, significant drop of the amorphous content of the coating at the shortest spray distance (200 mm) is due to the formation of the oxide. Oxide fraction of the coating at 200 mm spray distance is the highest due to the excess heat from the HVOF torch flame.

(2) As the fuel flow rate is increased, the amorphous content of the coatings is decreased. This is due to the facts that the oxide formation of the coatings has increased with increasing the HVOF jet temperature.

(3) The oxide phase formed in the coatings results from the exposure to high temperature during and after solidification of the droplets after spraying process as well as from the feedstock powders containing oxides. Therefore, it is necessary to consider both the critical cooling rate of the alloy for the formation of the amorphous phase and the oxidation resistance of the alloy at high temperature.

References

1. J. W. LUSTER, G. R. HEATH and P. A. KAMMER, *Materials and Manufacturing Processes* **11** (1996) 855.
2. A. BORISOVA, Y. BORISOV, V. KORZHYK and V. BOBRIK, in "Thermal Spraying: Current Status and Future Trends," edited by A. Ohmori (Kobe, Japan, 1995) p. 749.
3. K. KISHITAKE, H. ERA and F. OTSUBO, *J. Thermal Spray Technol.* **5** (1996) 145.
4. *Idem., ibid.* **5** (1996) 283.
5. H. MIURA, S. ISA and K. OMURO, *Trans. of the Japan Inst. of Metals* **15** (1984) 284.
6. H. J. KIM and Y. J. KIM, *J. of Mat. Sci.* **34** (1999) 29.
7. H. J. KIM, S. GROSSI and Y. G. KWEON, *Wear* **232** (1999) 51.
8. M. NAKAYAMA, H. ITO, R. NAKAMURA and M. TOH, in "Thermal Spraying: Current Status and Future Trends," edited by A. Ohmori (Kobe, Japan, 1995) p. 1063.
9. Y. BORISOV, V. BORISOV, V. KORZHYK, V. GOLNIK, E. LUGSCHEIDER and P. JOKIEL, in "Thermal Spray: Research, Design and Applications," edited by C. C. Berndt and T. F. Bernecki (Anaheim, CA, USA, 1993) p. 531.
10. A. INOUE, T. ZHANG and T. MASUMOTO, *J. Non-Crystalline Solids* **156–158** (1993) 473.
11. Y. J. KIM, R. BUSCH, W. L. JOHNSON, A. J. RULISON and W. K. RHIM, *Appl. Phys. Lett.* **65** (1994) 2136.
12. H. H. HNG, Y. LI, S. C. HG and C. K. ONG, *J. Non-Crystalline Solids* **208** (1996) 127.
13. K. M. LIM, H. J. KIM, Y. W. KIM and C. G. PARK, *J. Kor. Inst. Met. & Mater.* **38** (2000) 403.
14. A. INOUE, Y. KAWAMURA, T. SHIBATA, K. SASAMORI, *Mater. Trans. JIM* **37** (1986) 1337.
15. W. D. SWANK, J. R. FINCKE, D. C. HAGGARD, G. IRONS and R. BULLOCK, in "Thermal Spray Industrial Applications," edited by C. C. Berndt and S. Sampath (Boston, MA, USA, 1994) p. 319.
16. Z. ALTOUNIAN and J. O. STRON-OLSEN, in "Thermal Analysis in Metallurgy," edited by R. Shull and A. Joshi (TMS, Worrendale, PA, USA, 1992) p. 155.
17. P. T. VIANCO and J. C. M. LI, *J. of Non-Crystalline Solids* **107** (1989) 225.

Received 16 December 1999
and accepted 5 June 2000